A rewiring of the earliest immune events leading to T-cell mediated disease following intestinal microbial infection in a PINK1KO mouse model of Parkinson's disease

Sherilyn Junelle Recinto[1,6], Alexandra Kazanova[2,6], Hicham Bessaiah[2], Brendan Cordeiro[2], Sriparna Mukherjee[3,4,6], Shobina Premachandran[1], Adam MacDonald [1,6], Jessica Pei[2,6], Alexis Allot[1], Elia Afanasiev[1], Heidi M McBride[1,6], Louis-Eric Trudeau[3,4,6], Samantha Gruenheid[2,6]†, Jo Anne Stratton[1,6]†

[1]Dept. of Neurology and Neurosurgery, Montreal Neurological Institute-Hospital, McGill University, Montréal, QC, Canada
[2]Dept. of Microbiology and Immunology, McGill University, Montréal, QC, Canada
[3]Department of Neuroscience, Faculty of Medicine, Université de Montréal, Montréal, QC, Canada
[4]Dept. of Pharmacology and Physiology, Faculty of Medicine, Université de Montréal, Montréal, QC, Canada
[5]Dept. of Pathology and Cellular biology, Faculty of Medicine, Université de Montréal, Montréal, QC, Canada
[6]Aligning Science Across Parkinson's (ASAP) Collaborative Research Network, Chevy Chase, MD 20815, USA

†Corresponding author

Jo Anne Stratton	Samantha Gruenheid
McGill University	McGill University
H3A 2B4, QC, Canada	H3A 2B4, QC, Canada
T: +1 514 224 2558	T: +1 514 398 2138
E: jo.stratton@mcgill.ca	E: sam.gruenheid@mcgill.ca

Running title: A rewiring of the earliest immune events leading to T-cell mediated disease following intestinal infection in a PINK1KO mouse model of Parkinson's disease

Licensing: CC-BY 4.0 International license for the copywriter

Keywords: Immunity, inflammation, infection, mitochondria, PINK1 kinase, myeloid cells, gut, Parkinson's disease, single cell RNAsequencing

Abstract

Parkinson's disease (PD) is characterized by a protracted period of non-motor symptoms, including gastrointestinal (GI) dysfunction, which can precede the development of cardinal motor dysfunction by decades. This long prodrome of disease is highly suggestive of immune cell involvement in the initiation of disease, but currently the field lacks robust modeling systems to study such mechanisms. Pathology may be first initiated in the periphery due to environmental triggers, such as pathogens that enter the GI tract in genetically predisposed individuals. Our group has developed GI-targeted pathogen-induced PD mouse modeling systems (in PINK1 KO mice with gram negative bacterial infections) and found that T cells are a major player in driving PD-like motor symptoms at late stages following infection. Herein, we now map the initiating immune events at the site of infection at the earliest stages with the goal of shedding light on the earliest mechanisms triggering T cell-mediated pathological processes relevant to PD. Using unbiased single cell sequencing, we demonstrate that myeloid cells are the earliest dysregulated immune cell type in PINK1 KO infected mice (at 1-week post-infection) followed by a dysregulated T cell response shortly after (at 2 weeks post-infection). We find that these myeloid cells have an enhanced proinflammatory profile, are more mature, and develop enhanced capacity for antigen presentation. Using unbiased prediction analysis, our data suggests that cytotoxic T cells and myeloid cells are particularly poised for interacting with each other, and we identify possible direct cell-cell interaction pathways that might be implicated. How or if these early aberrant immune responses play a key role in initiating PD autoimmunity is the subject of further investigation.

Introduction

Parkinson's disease (PD) is a highly prevalent, age-associated progressive neurodegenerative disorder characterized by a long prodromal phase of non-motor symptoms (such as hyposmia, constipation, sleep disruption and anxiety), followed by motor functional deficits (such as bradykinesia, tremor and rigidity) which is associated with loss of dopaminergic neurons in the substantia nigra pars compacta of the midbrain (Braak et al., 2003; Tysnes & Storstein, 2017). Given the extensive prodromal period, it suggests that disease initiating mechanisms may occur early in one's life, but the disease remains relatively dormant and largely asymptomatic until the onset of overt symptoms as one ages, with the average age of PD diagnosis being 66 (*Parkinson's disease: Prevalence, diagnosis and impact*, 2015).

Inflammation has been identified as a major risk factor for PD. Most PD patients are subject to a "body-first" pattern of nervous system pathology which is consistent with peripheral inflammation being involved in early disease (Chen et al., 2022). But exactly how PD genes might be involved in peripheral inflammation in PD remains unclear. For example, in the case of *PTEN-induced kinase 1* (PINK1), a PD associated serine/threonine kinase, the traditional view is that this kinase becomes dysregulated in PD resulting in disrupted mitophagy resulting in dopaminergic neuron death critical for PD pathogenesis (Heo et al., 2015; Lazarou et al., 2015; Pickrell & Youle, 2015). But there are critical roles for PINK1 that are mitophagy-independent. Our group previously showed that PINK1 represses immune responses independent of mitophagy, rather through disinhibition of mitochondrial-derived vesicle (MDV) formation which carries proteins to late endosomes, where they are further processed, typically for degradation (Matheoud et al., 2016). In the case of PINK1 loss, MDV transport to the endosomal compartments is heightened in dendritic cells undergoing cellular stress which resulted in the processing and presentation of mitochondrial peptides/antigens via MHCI, referred to as mitochondrial antigen presentation (MitAP). With MitAP occurring in the periphery, it is possible that naïve T-cells become educated against these self-peptides. Indeed, we have previously shown that elevated MitAP in PINK1 KO dendritic cells leads to the establishment of peripheral mitochondrial antigen-specific T cells, which can later access the brain and cause dopaminergic neurodegeneration (Kazanova et al., 2024; Matheoud et al., 2019). Others have also suggested a role for PINK1 in modulating innate immunity induced by oxidative stress and viral infection (Oh et al., 2024; Sliter et al., 2018; Zhou et al., 2019).

We have clearly demonstrated that intestinal infection with Gram-negative bacteria (*Citrobacter rodentium*) (Matheoud et al., 2019) in PINK1KO mice leads to antigen-specific T-cell autoreactivity. Critically, with aging and repeated infections, these mice later develop L-DOPA reversible PD-like motor impairments. Now, we have recently also discovered a similar phenomenon using a major PD-associated human-relevant pathogen (*Helicobacter pylori*), where autoreactive CD8+ T cell appear to drive PD-like motor phenotypes following GI infection in genetically predisposed rodents (Kazanova et al., 2024). Importantly, adoptive transfer of mitochondrial antigen-specific CD8+ T

cells was sufficient to induce similar motor impairments in wild-type mice which directly implicates autoimmunity as a causal mechanism of PD (Elemeery et al., 2024). Together, these data provide proof of concept that peripheral infections can lead to motor symptoms in genetically susceptible models of PD. We hypothesized that autoimmune mechanisms driven by T cells play a critical role in the initiation of PD which is first initiated by a dysregulated immune pathway at the earliest prodromal stages of disease. It remains unclear what early immune cascades are orchestrating an environment critical for the development of cytotoxic T cells capable of attacking the brain.

A pressing challenge to interrogate the initiating mechanisms of PD is a lack of clinically relevant “natural” models where the earliest stages of disease can be appropriately studied. To overcome this, there have been efforts to better develop models that trigger the natural course of PD development (Challis et al., 2020; Chandra et al., 2023; Kim et al., 2019; Matheoud et al., 2019; Sampson et al., 2020; Sampson et al., 2016; M. F. Sun et al., 2018; Zhong et al., 2021). Indeed, GI tract-initiated models of PD can recapitulate many early features of prodromal PD, such as constipation (Sampson et al., 2020; Sampson et al., 2016). There is accumulating evidence for a strong association between PD and GI disturbances, including intestinal inflammation. Analyses of immune profiles in the stools of PD patients demonstrate higher levels of inflammatory mediators suggestive of GI inflammation (Fan et al., 2024; Hor et al., 2022; Houser et al., 2018; Mulak et al., 2019; Schwiertz et al., 2018). Clinical studies further reveal that people with inflammatory bowel disease and GI infections have an increased risk of developing PD later in life (Fu et al., 2020; Houser et al., 2018; Lee et al., 2021; Liu et al., 2003; Nerius et al., 2020; Shen et al., 2017). Understanding the immune mechanisms that initiate disease early in the periphery at the cell/molecular level will address a major knowledge gap that hinders the development of diagnostic and therapeutic approaches to stop the onset of motor impairment at early steps of the disease before irreversible neuron death.

By exploiting our established model, we aimed to provide an in-depth characterisation of the initiating immune events in the gut mediated by PINK1 deficiency. We determine that intestinal infection in PINK1 KO mice provokes early immune dysregulation in the colon marked by the promotion of proinflammatory myeloid cell differentiation and an increased capacity for antigen presentation. This process was followed by the activation and expansion of intestinal CD8+ T cells, which we postulate is due to mis-presentation of self-peptides, laying the foundation for autoimmunity later in life. Ultimately, mapping the earliest immune-mediated mechanisms in PD will be pivotal to develop better biomarkers and effective therapeutic targeting, prior to the development of irreversible neuronal damage.

Results

Single cell RNAseq of the colon unveils a role of PINK1 within the immune cell compartment at the earliest stages following infection

We have previously described that repeated infection of PINK1 KO mice with mouse intestinal gram-negative pathogen *C. rodentium* via gavage induces L-DOPA reversible motor symptoms 16- to 24-weeks later (Matheoud et al., 2019). Despite clear evidence for the role of autoreactive CD8+ T cells in the neurodegenerative process within the brain (Elemeery et al., 2024; Kazanova et al., 2024), it is unknown how this is instigated. The phases of *C. rodentium* infection subsequent to its establishment in the colon is well described, and includes bacterial expansion (by 1 week), steady-state (1-2 weeks) and clearance (2+ weeks). This immune response is governed by several players of innate and adaptive immunity, including early myeloid cell responses driven by dendritic cells (DCs) then ultimately the engagement of type I and interleukin 17 (IL17)-producing T helper cells (Th1 and Th17, respectively) for complete clearance of the infection (Mullineaux-Sanders et al., 2019).

We first employed an indirect, non-invasive approach using fecal analysis to evaluate whether there was any evidence for enhanced inflammation in PINK1 KO mice at any point over time. We used enzyme-linked immunosorbent assay (ELISA) to detect lipocalin-2 (LCN2), which is highly expressed by activated innate immune cells and epithelium, and often used as indicator of intestinal inflammation (Chassaing et al., 2012; Stallhofer et al., 2015) (Fig. 1A). We noted a progressive increase in LCN2 concentration over time which reached significance in wild type and PINK1 KO mice at 2- and 4- w.p.i. compared to uninfected mice. Importantly, there was also significantly more LCN2 in PINK1 KO infected mice compared to wild type infected mice at these time points.

To gain insight into PINK1-mediated alterations in the intestinal immune landscape, we then performed single cell RNAseq using 10X droplet-based microfluidics technology in FACS-sorted whole cell colonic lamina propria cells (Fig 1B). Briefly, we prepared gene expression libraries from wild type and PINK1 KO infected mice along with uninfected control groups at 1- and 2-w.p.i. (Fig. 1C). Subsequent to the integration of our datasets employing standard parameters in *Seurat* (Butler et al., 2018), we annotated all immune cell types using identity markers curated from the literature for each cell cluster (Fig. 1D, E). By comparing WT and PINK1 KO datasets in each distinct condition (uninfected control, 1-w.p.i. and 2-w.p.i.), we determined transcriptional regulation driven by PINK1 in specific immune cell types in response to intestinal infection. As shown in Fig. 2A, we did not observe obvious genotype-dependent alterations in cell cluster identities in each

condition, although as expected, we noticed a larger population of granulocytes at 1-and 2- w.p.i. in both genotypes compared to the uninfected groups. Meanwhile, CD4+ and CD8+ T cell subtypes became more prominent at 2-w.p.i. These changes are consistent with the involvement of innate and adaptive immunity in bacterial clearance at these timepoints (Mullineaux-Sanders et al., 2019). Next, we performed differential gene expression analyses between PINK1 KO and wild type mice. The heatmap in Fig. 2B displays the number of genes that were either significantly upregulated (red) or downregulated (blue) in each immune cell types of PINK1 KO mice (adjusted p-values < 0.05 using non-parametric Wilcoxon rank sum test with Bonferroni correction applied to evaluate significance). The largest regulation was within the myeloid cell compartment (Fig. 2B). We found high transcriptional changes in monocytes/macrophages and dendritic cells at 1-w.p.i., followed by CD4+ Th1 and Th17 as well as CD8+ cytotoxic T cells (Tc1) at 2-w.p.i. Together, these results indicate that PINK1 loss impairs intestinal immune responses to gram-negative bacterial infection leading to exacerbated inflammation early after infection, well before motor symptoms arise.

Higher proportions of effector T cells depicting proinflammatory and cytotoxic characteristics are present at 2-weeks post-infection in the colon of PINK1 KO mice

Effector CD4+ and CD8+ T cell subtypes that appear to be more abundant in peripheral blood, cerebrospinal fluid and brains of PD patients are now widely being investigated due to their proinflammatory and cytotoxic profiles (Bhatia et al., 2021; Galiano-Landeira et al., 2020; Jakubiak et al., 2024; Kimura et al., 2024; Lindestam Arlehamn et al., 2020; Schröder et al., 2018; Sulzer et al., 2017; Wang et al., 2021; Williams et al., 2024). Previous findings by our group indeed points to the proliferation of autoreactive CD8+ T cells as a prerequisite for driving *late* CNS-related pathological process via major histocompatibility class I (MHCI)-mediated antigen presentation by dendritic cells in the spleen (Kazanova et al., 2024; Matheoud et al., 2019; Matheoud et al., 2016). However, it is unknown if PINK1 loss also potentiates the recruitment or expansion of effector T cells and alters their expression profile in the gut at the earliest stages of disease.

To address this, we first dissected the behaviour of CD4+ and CD8+ T cells by performing trajectory analyses at 2-w.p.i. using *Slingshot (Street et al., 2018)* (Fig. 3A). This bioinformatic tool can identify distinct T cell lineages based on gene expression changes between cell clusters generated by unsupervised hierarchal clustering. Depending on the position in a given trajectory, a pseudotime value is assigned to a cell with increasing number, the further it is from the origin of the lineage which, in this case, is defined as naïve T cells (Tn). In CD4+ T cells, four lineages were obtained starting from Tn towards different effector T cell subtypes: 1) Th1 to helper type 2 (Th2) and IL17-producing Th2 cells; 2) Th1 to resident memory cells (Trm); 3) Th1 to Th17 cells; and 4) Treg (data not shown). Considering that Th1 and Th17 gene expression was most regulated within the CD4+ T cell populations (Fig. 2B), we probed this lineage transition to examine the frequency of these proinflammatory effector T cells (Fig. 3A, upper panel). PINK1 KO mice exhibited higher Tn to effector T cell transitions for both

Th1 and Th17 compared to wild type, the Tn-to-Th1 transition was most obvious with a three-fold higher ratio (Fig. 3B, upper panel). Pseudotime analyses of CD8+ T cell population revealed a single trajectory from Tn to cytotoxic CD8 Tc1 to Trm cells (Fig. 3A, lower panel). Proportional analyses demonstrated that CD8+ T cell differentiation was greater in PINK1 KO compared to wild type, with a four-fold increase in Tn-to-Tc1 ratio and Tn-to-Trm ratio (Fig. 3B, lower panel).

Given the expansion of Th1 and Tc1 populations in PINK1KO mice, and the high degree of gene regulation in these populations (Fig. 2B), we conducted pathway enrichment analyses using Gene Ontological (GO) terms to determine the top 40 biological processes that were associated with differentially expressed genes (DEGs) that were significant between PINK1 KO and WT in each of these T cell subtypes. A large number of GO terms were conserved across T cell types which related to the activation of adaptive immunity (Fig. 3C, 3D). Amongst them were T cell differentiation, cellular response to interleukin-4 (which is imperative in shaping T cell responses), leukocyte cell-cell adhesion, T cell-mediated cytotoxicity and cell killing. We also highlight some DEGs that were driving these GO terms (Fig. 3C, 3D), which include activation/suppressive markers such as *Stat3*, *Xbp1*, *Cd40lg*, *Il7r*, *Pdcd1*, as well as genes encoding tumor necrosis factor (TNF) ligand superfamilies (*Tnfrsf4*, *Tnfsf8*), C-C chemokine receptors and cytokines (*Ccr1*, *Ccr2*, *Ccr5*, *Ccl8*) and genes involved in cytotoxic T cell function (*Klrk1*, *Klrc1*, *Prf1*). Overall, PINK1-mediated immune dysregulation in the gut contributes to the expansion of proinflammatory and cytotoxic effector T cell subtypes early in disease.

Proinflammatory myeloid cells with enhanced antigen presentation capacity are present at 1-week post-infection in the colon of PINK1 KO mice

In contrast to T cell reactivity, which we deem pivotal for late-stage neurodegeneration, the role of myeloid cell populations in PD is less clear. About 80% of patients with REM-sleep behaviour disorder (RBD) eventually receive a PD diagnosis (Schenck et al., 2013), making this patient group ideal for studying the prodrome of PD. Studies of the peripheral blood from RBD patients demonstrates abnormal patterns of gene signatures of monocytes which inversely correlates with cognitive/motor performance & midbrain dopamine function in patients (Farmen et al., 2021; Wang et al., 2022; Wijeyekoon et al., 2020). This suggests that monocyte features may be an important early biomarker of disease activity, but what monocyte-related molecular pathways might be involved in the initiation of disease is not known.

Interestingly, our infection-induced PD model indeed substantiates the involvement of myeloid cells at the earliest stages of disease whereby the highest number of DEGs were found within the intestinal monocytes/macrophages and dendritic cell populations at 1-w.p.i. (Fig 2B). The top 40 GO terms associated with these DEGs in macrophages/monocytes illustrates dysregulated inflammatory pathways, such as leukocyte cell-cell adhesion, T cell proliferation and activation, cell chemotaxis/migration, cellular response to lipopolysaccharide (LPS) and cytokine-

mediated signaling pathway (Fig. 4A-C). To validate PINK1-driven myeloid cell changes, we isolated $CD45^{+}CD11b^{+}F4/80^{-}Ly6C^{high}$ monocytes from the colonic lamina propria of PINK1 KO and wild type mice at 1-w.p.i. by flow-activated cell sorting (FACS) along with uninfected control groups (Fig. 5A). We observed significantly altered expression of key DEGs suggestive of enhanced proinflammatory responses in intestinal monocytes of PINK1 KO infected mice, including lipocalin-2 (*Lcn2*), serum amyloid a3 (*Saa3*), aconitate decarboxylase 1 (*Acod1*), toll-like receptor 2 (*Tlr2*), hypoxia-inducible factor 1 alpha (*Hif1*α) and interleukin-10 (*Il10*) (Fig. 5B).

In recent years, the complex role of PINK1 across different contexts and cell types is beginning to unfold (Dai et al., 2021). Not only has PINK1 been implicated in myeloid cell activation, its ubiquitous expression in non-immune cell types has also been involved in cell fate decisions (Cairns et al., 2024; S. Y. Lee et al., 2021). Consequently, we delved deeper into the myeloid cell lineage at 1-w.p.i. and performed unsupervised clustering on these cells (generating higher resolution principal component analyses) to identify monocytes distinct from macrophages and dendritic cells. We then analyzed the differential trajectories in the myeloid cell lineage using the aforementioned methods, providing monocytes as the root (Fig. 4D). In keeping with the literature, we denoted two distinct lineages in both wild type and PINK1 KO mice emerging from monocytes to either macrophages (MΦ) or dendritic cells (DC) whereby each cell within a particular lineage is assigned a pseudotime value; the higher it is, the higher the propensity to commit to the specified lineage. To determine the likelihood of intestinal monocytes to differentiate into mature myeloid cells, we quantified the proportions of monocytes from wild type and PINK1 KO mice at 1-w.p.i. with low or high pseudotime values defined as [0, 10] and [10, 20], respectively (given the majority of monocytes fall with the range of 0 to 20) (Fig. 4D). This suggests that PINK1 KO monocytes have a greater tendency to commit in becoming proinflammatory, professional antigen-presenting cells as evidenced by a higher ratio of MΦ or DC-like to immature ratios in PINK1 KO infected mice compared to wild type (Fig. 4E, 4F). The elevated protein expression of CD11b and CD11c, which are cell surface markers of MΦ and DC populations, in intestinal $Ly6C^{high}$ monocytes from PINK1 KO infected mice, further attests to the increased differentiation capacity of PINK1 KO monocytes when activated (Fig. 5C).

Myeloid and CD8+ T cells are poised for direct cell-cell contact mediated interactions in the colon of infected mice

We have previously shown that when the adaptive immune response goes awry in the context of PD, it is likely attributed to deregulated antigen presentation triggering CD8+ T cells that mount a cytotoxic response against these self-antigens (Elemeery et al., 2024; Matheoud et al., 2019; Matheoud et al., 2016). Intriguingly, by conducting cell-cell interaction analyses using *CellChat* (Jin et al., 2021), we bioinformatically uncovered that myeloid and CD8+ T cells have the strongest interactions based on the incoming/outgoing signals received or sent within the immune milieu of the gut (Fig. 6A). Moreover, given that myeloid cells (monocytes/macrophages and dendritic cells) are consistently the strongest signal senders at both 1- and 2-w.p.i., we assessed their

communication to all immune cell types following infection. Notable, there were minimal differences in the pathways involved in various cell-cell interactions between wild type and PINK1 KO mice (Fig. 6B). Despite this, we discerned multiple pathways pertaining to direct cell-cell contact-mediated myeloid cell interactions in both genotypes, and found that CD8 Tc1 was a major cell type receiving signals. This involved signalling pathways relating to antigen presentation, such as major histocompatibility complexes (MHC), co-stimulatory molecules (CD86 and CD80), programmed death-ligand 1 (PD-L1) and intercellular adhesion molecule 1 (ICAM1) amongst other highlighted in Fig. 6B. As such, we next examined the expression of key molecules in the antigen presentation pathway using flow cytometry of intestinal Ly6C^{high} monocytes following infection of wild type and PINK1 KO mice. Indeed, we observed increased levels of MHC, CD86, PDL1 and ICAM1 that participate in the pathways highlighted above in PINK1 KO monocytes (Fig. 6C).

Discussion

Given the multifaceted nature of PD etiology, it is important we interrogate genetic and environmental triggers of disease, including how a dysregulation in the immune system can drive pathophysiological processes implicated in disease initiation and progression. In our current study, we have characterized a key model that is geared to study the earliest features of disease driven by genetic-environmental interactions. This has uncovered a dysregulation in the myeloid cell compartment at the initial stages of disease potentially instigating enhanced antigen presentation and mitochondrial antigen-specific CD8+ T cell-mediated autoimmune changes observed at late-stages of PD.

In line with numerous reports highlighting the role of other genes associated with familial PD in inflammation (Fahmy et al., 2023; Fava et al., 2019; Härtlova et al., 2018; Li et al., 2019; Liu et al., 2017; Nguyen et al., 2023; Xin et al., 2018), PINK1 has been shown to acquire pleiotropic effects in innate immunity (Jin et al., 2023; Oh et al., 2024; Sliter et al., 2018; L. Sun et al., 2018; Zhou et al., 2019). Albeit, whether PINK1-driven changes in inflammatory signaling instigate early disease process in PD remained elusive. We discovered that the myeloid cell lineage exhibits the most substantial dysregulation at the initial stage of our infection-induced model. We further reveal an amplified proinflammatory response in monocytes of PINK1 KO infected mice, including upregulation of HIF1α. Consistent with this, a prior study conducted by Requejo-Aguilar *et al.* demonstrated that deletion of PINK1 in non-immune cells resulted in the regulation of glucose metabolism reprogramming to sustain cell proliferation requiring increases in ROS production, which necessitates the activation of HIF1α signaling (Requejo-Aguilar et al., 2014). Our data suggests an early HIF1α-mediated metabolic alteration in activated PINK1 KO monocytes, which is consistent with what is observed in monocytes from peripheral blood of RBD patients. Indeed, these patients display elevated levels of mitochondrial ROS associated with a concomitant increase in glycolysis (Smith et al., 2018). Other features of RBD monocytes include regulation of

human leukocyte antigen (HLA)-DR expression which correlates with worse cognitive and motor performance (Wijeyekoon et al., 2020), while changes in TLR4 expression inversely correlates with midbrain dopamine function measured by ^{18}F-DOPA positron emission tomography (PET) imaging (Farmen et al., 2021). This data is consistent with our data demonstrating differential expression of major histocompatibility complexes and toll-like receptors in intestinal monocytes of PINK1 KO infected mice.

Cellular roles of PINK1 are context-dependent and operate in response to a distinct type of stress since previous data shows conflicting results as to whether PINK1 mitigates or promotes inflammation (Oh et al., 2024; Sliter et al., 2018; L. Sun et al., 2018; Williams et al., 2024; Zhou et al., 2019). Sliter *et al.,* reported that PINK1 KO mice under mitochondrial stress display excessive systemic levels of proinflammatory cytokines, interleukin 6 and β-interferon via the activation of the cGAS-STING signaling pathway (Sliter et al., 2018). A congruent *in-vitro* study of human skin cells following varicella zoster viral infection elucidated PINK1-dependent attenuation of STING-mediated interferon responses (Oh et al., 2024). By contrast, PINK1 was shown to induce retinoic-acid-inducible gene I (RIG-I)-like receptors-mediated antiviral immunity in peritoneal macrophages (Zhou et al., 2019). In our intestinal bacterial infection-induced PD model, we provide evidence for a negative regulation of PINK1 in early responses of myeloid cells. It is still unclear if this PINK1-driven dysregulation in myeloid cells directly hinders neuronal health both in the periphery and the CNS or indirectly through its interaction with cytotoxic T cells. *Sun et al.,* previously depicted that PINK1 deletion in microglia promoted neuroinflammatory milieu conducive to neuronal death *in vitro (L. Sun et al., 2018)*. Understanding the mechanisms for how PINK1 loss potentiates inflammatory responses in myeloid cells and the repercussions on dopaminergic neurons will be crucial to targeting immune-mediated pathological processes implicated at disease onset.

The contribution of PINK1 in inflammation has largely been attributed to its role in regulating mitophagy. During cellular stress, this serine/threonine kinase together with another PD-associated protein, E3 ubiquitin ligase Parkin are stabilized at the surface of damaged mitochondria critical for mitophagy to occur. In the absence of PINK1/Parkin, impaired mitophagy occurs and is traditionally viewed as the putative mechanism in PD that governs dopaminergic neuron death (Heo et al., 2015; Lazarou et al., 2015; Pickrell & Youle, 2015). Recent work elucidated rather a role of PINK1-driven mitophagy in modulating innate immunity induced by oxidative stress and viral infection (Oh et al., 2024; Sliter et al., 2018; Zhou et al., 2019). Interestingly, our group previously showed that PINK1 represses immune responses independent of mitophagy, but through disinhibition of mitochondrial-derived vesicle (MDV) formation which carries proteins to late endosomes, where they are further processed, typically for degradation (Matheoud et al., 2016). In the case of PINK1 loss, MDV transport to the endosomal compartments is heightened in dendritic cells undergoing cellular stress which resulted in the processing and presentation of mitochondrial peptides/antigens via MHCI, referred to as MitAP. With MitAP occurring in the periphery, it is possible that naïve T-cells become educated against these self-peptides. Indeed, we have previously shown that elevated MitAP in PINK1 KO dendritic cells leads to the establishment of peripheral mitochondrial

antigen-specific T cells, which can later access the brain and cause dopaminergic neurodegeneration (Kazanova et al., 2024; Matheoud et al., 2019). Critically, we will determine whether this could be a direct attack, given we and others have already described an increase in cell surface expression of MHCI in dopaminergic neurons under inflammatory states (Cebrián et al., 2014; Matheoud et al., 2019), rendering these neurons susceptible for direct autoimmune T cell-mediated degeneration. Importantly, our current study further reveals that deregulated antigen presentation occurs at the earliest stage of disease as evidenced by upregulation of MHC molecules and co-stimulatory ligands, including CD86 and ICAM1, in intestinal PINK1 KO monocytes. Future work aims to unravel how or if these early aberrant immune responses play a key role in initiating PD autoimmunity.

Following acute *C.rodentium* infection, myeloid cells in the gut are predicted to interact the most with CD8+ Tc1 cells via antigen presentation pathways, which may poise this process to go in awry in the absence of functional PINK1. The activation of intestinal CD8+ Tc1 cells in PINK1 KO mice during the prodrome is further illustrated by upregulation of *Stat3* and *Ccr5*. Prior studies demonstrate that CCR5 overexpression associates with the activation of the JAK/STAT signaling pathway in human CD4+ T cells (Wang et al., 2024); and accumulation of CCR5 at the immunological synapse engender more robust T cell-APC interactions (Contento et al., 2008). Interestingly, intestinal CD8+ Tc1 cells in PINK1 KO infected mice also display elevated levels of T cell exhaustion markers, including *Pdcd1*, *Ikzf2* and *Il2rb* concomitant with increased expression of cytotoxic mediator perforin (*Prf1*). Not only are effector CD8+ T cells expanding in the gut at an early stage in our infection-induced PD model, but we also noted that these cells have exacerbated cytotoxic functions that may potentially result in exhaustive features. Of note, a related infection model showed that mitochondrial antigen-specific CD8+ T cells express the exhaustion marker PD-1 (Kazanova et al., 2024) consistent with this notion. Consequently, further characterization of naturally occurring mitochondrial proteins processed and presented through the PINK1-controlled MDV pathway is warranted and will open novel avenues catering early detection and intervention in PD.

Ultimately, mapping the earliest immune-mediated mechanisms in PD will be pivotal to develop better biomarkers and effective therapeutic targeting, prior to the development of irreversible neuronal damage. How or if these early aberrant immune responses play a key role in initiating PD autoimmunity is the subject of further investigation.

Methods

Mice

DAT-Ires-Cre (RRID:IMSR_JAX:006660) mice were bred with Ai9 mice (RRID: IMSR_JAX:007909) to induce the expression of tdTomato in DAT-expressing cells (DAT- tdTomato) then were crossed with PINK1-deficient (PINK1 KO) mice in a mixed B6.129 background. Adult DAT-Cre-tdTomato wild type and PINK1 KO mice (both sexes) were utilized in the present study. Mice were housed under specific pathogen-free conditions, given water and food ad libitum. Studies were approved by the

Université de Montréal and McGill University Animal Care and Use Committee (CDEA). CDEA guidelines on the ethical use and care of animals were followed.

Infection with *C.rodentium*

As done previously (Matheoud et al., 2019), mice were infected with chloramphenicol-resistant *C. rodentium* (4×10^{-9} CFU) by oral gavage. To monitor bacterial burden, faeces were collected from each mouse, weighed, dissociated in PBS, serial-diluted and plated on chloramphenicol MacConkey agar Petri plates. Petri plates were incubated at 37 °C overnight to allow colony growth, which were counted the following day. Final counts were measured as CFU g^{-1} of faeces. Faecal collection occurred on 1-, 2- and 4-weeks-post- infection (w.p.i.) to confirm $\geq 10^7$ CFU/g infection rates (~80% of infected mice achieved this rate and were included in the study).

Enzyme-linked immunosorbent assay

Faecal samples were suspended in PBS plus 0.1% Tween20 at a ratio of 100 mg of faeces per millilitre. To isolate the supernatants, samples were vortexed for 20 min before centrifugation at 13,000 rpm at 4°C. ELISA was performed using the mouse Lipocalin-2 DuoSet kit (R&D Systems) as per manufacturer's instructions. In brief, collected supernatants were applied to a 96-well plate pre-coated with Lipocalin-2 capture antibody, washed three times with PBS plus 0.05% Tween20, treated with the detection antibody, washed three times, treated with streptavidin–HRP, washed three more times, and developed with a 1:1 ratio of hydrogen peroxide and tetramethylbenzidine. The optical density of the plates was read at 450 nm.

Colonic lamina propria cell preparation

Colons were dissected then fecal material was flushed with an 18G needle and adipose tissue was removed. Colon was then cut longitudinally and then chopped into sections of 1-2 cm in length. To separate the mucosal epithelium, intestinal tissue sections were incubated in 2 mM EDTA at 37°C for 15 mins followed by vigorous manual shaking three times until cellular suspension appears dense and cloudy. Remaining intestinal tissue sections (consisting of the lamina propria (LP) cells) were then collected and enzymatically dissociated with 2:1 ratio of collagenase IV to DNAse I at 37°C for 30 mins followed by vigorously vortexing. Cellular suspension was then collected through a 70 μm cell strainer. A subsequent similar enzymatic digestion is necessary to completely dissociate intestinal tissue and release the whole lamina propria cells, which is then pooled with the first dissociation. Cells were spun down at 1500 rpm at 4°C for 7 mins at the end of each enzymatic digestion then pellet was resuspended in PBS supplemented with 1% fetal bovine serum (FBS). Percentage of viability was assessed by flow cytometry and obtained at an average of 60%. Cells were subject to downstream experiments, including cell surface staining to acquire cell profile as well as cell sorting for qPCR and single-cell RNAseq.

Once separated, the mucosal epithelium was processed independently for single-cell RNAseq. Briefly, the cloudy cellular suspension containing the crypts was further dissociated into single cells by resuspending in TrypLe using 21G needle followed by 10 mins incubation at 37°C. The reaction was neutralized with basal media (Advanced

DMEM F/12 supplemented with 10% FBS). Cellular suspension was then collected through 40 μm cell strainer and spun down at 900 rpm at 4°C for 5 mins. The pellet was resuspended in PBS supplemented with 1% FBS. Percentage of viability was assessed by flow cytometry and obtained at an average of 40%. Finally, live single cells were collected by FACS.

Bone-marrow-derived myeloid cell differentiation

Sex-paired cohorts of male or female mice at 6 to 12 weeks of age were euthanized and bone marrow progenitor cells were flushed through a 25G needle from both femurs. Bone marrow cells were further dissociated by passing through 18G needle and collected through 70 μm cell strainer. Progenitors were then differentiated in complete basal medium (RPMI supplemented with 10% FBS, 1% antibiotic/antimycotic and GlutaMAX Supplement 1X) with 20 ng/mL recombinant mouse M-CSF for at least 7 days or recombinant mouse GM-CSF for at least 9 days to generate bone marrow-derived macrophages (BMDM) or dendritic cells (BMDC), respectively. Media changes were completed every 2-3 days. Matured cells were harvested after 500ng/mL LPS treatment overnight.

Flow cytometry

Following isolation, cells resuspended in PBS were stained using eBioscience fixable viability dye coupled with either Zombie Red (for LP) or eFluor 506 (for BMDM) (Invitrogen Cat# 65-0866-14) for 20 mins on ice, in the dark. Prior to washes with FACS buffer (PBS supplemented with 2% FBS and 1 mM EDTA), cells were spun down at 400 xg at 4°C for 5 mins. Fc receptors were then blocked with anti-mouse CD16/CD32 (Invitrogen, Cat# 14-01061-86) along with extracellular staining with a mixture of conjugated antibodies in FACS buffer (1:250 for LP cells; concentrations indicated in the table below for BMDM/C) for 30 mins on ice, in the dark. The antibodies used are shown in Table 1 and 2. After multiple washes, cells were resuspended in FACS buffer then acquired using either Fortessa (for LP cells) and Attune NxT (for BMDM/C). For sorting live single cells, FACS Aria was used instead. Appropriate controls were applied such as compensation beads and fluorescence minus one (FMOs).

Table 1: Cell surface staining of lamina propria (LP) cells

Antigen	Fluorophore
CD45	BV750
CD11b	APC Fire 810
Ly6C	PerCP-Cy5.5
F4/80	APC
CD11c	PE Fire 810
MHCII	APC-Cy7
CD86	Alexa Fluor 700
PD-L1	BV421
ICAM1	FITC

Antigen	Fluorophore	Concentrations

CD11b	PerCP-Cy5.5	1:300
F4/80	PE-Texas Red	1:300
CD11c	APC e780	1:200
MHCII	PE-Cy7	1:500
MHCI	PE	1:300
CD86	FITC	1:200
CD80	BV650	1:200

Table 2: Cell surface staining of BMDM/C

Quantitative reverse transcription PCR

RNA was extracted using the RNeasy mini kit (Qiagen) as instructed by the manufacturer. High-Capacity cDNA Reverse Transcription Kit (Applied Biosystems) was then used for reverse transcription to generate cDNA which was used for real-time quantitative PCR (qPCR) via TaqMan assays on a QuantStudio™ 5 real-time PCR system (Thermo Fisher Scientific). The $2^{-\Delta\Delta Ct}$ method was used to analyse the data using *Actb* or *Gapdh* as controls.

Single-cell library preparation and analysis

Live cells were prepared for single-cell sequencing at final concentration of 1000 cells/µL. All cells were processed according to 10X Genomics Chromium Single Cell 3' Reagent Guidelines (https://support.10xgenomics.com/single-cell-gene-expression). Briefly, cells were partitioned into nanoliter-scale Gel Bead-In-EMulsions (GEMs) using 10X GemCode Technology. Primers containing (i) an Illumina R1 sequence, (ii) a 16 bp 10x barcode, (iii) a 10 bp Unique Molecular Identifier (UMI) and (iv) a poly-dT primer sequence were incubated with partitioned cells resulting in barcoded, full-length cDNA from poly- adenylated mRNA. Silane magnetic beads were used to remove leftover biochemical reagents/primers, then cDNA was amplified by PCR. Enzymatic fragmentation and size selection was used to optimize cDNA amplicon size prior to library construction. R1 (read 1 primer sequence) were added during GEM incubation, whereas P5, P7, a sample index (i7), and R2 (read 2 primer sequence) were added during library construction via end repair, A-tailing, adaptor ligation and PCR. Quality control and quantification was performed using an Agilent Bioanalyzer High Sensitivity chip. Sequencing was performed using NovaSeq 6000 S4 PE 100bp, which resulted in a read depth of ~20 000 reads/cell. Reads were processed using the 10X Genomics Cell Ranger Single Cell 2.0.0 pipeline (RRID:SCR_017344, https://support.10xgenomics.com/single-cell-gene-expression/software/pipelines/latest/what-is- cell-ranger) with default and recommended

parameters, as previously described (Zheng et al., 2017). FASTQs generated from sequencing output were aligned to the mouse GRCm38 reference genome using the STAR algorithm 2.7.3a (RRID:SCR_004463, http://code.google.com/p/rna-star/) (Rahmani et al., 2020). Next, gene-barcode matrices were generated for each individual sample by counting unique molecular identifiers (UMIs) and filtering non-cell associated barcodes. This output was then imported into the Seurat v4.9.9.9039 R toolkit v.4.2.1 (for quality control and downstream analysis of our single cell RNAseq experiment (Macosko et al., 2015). All functions were run with default parameters, unless specified otherwise. Low quality cells (<200 genes/cell and >5 % of mitochondrial genes) were excluded from the overall experiment. Gene expression was log normalized to a scale factor of 10 000.

Statistical analysis

Statistical analyses were performed using GraphPad Prism 5.0 software. A two-way ANOVA was used to compare the mean of three or more groups of data. *P*-values were adjusted using Tukey's multiple comparison test. Mean and standard error of the mean (SEM) of biological replicates (*n*) are plotted in all graphs and indicated in the Figure legends. *P-value* < 0.05 was considered statistically significant.

Illustrations

Graphical abstract and experimental designs illustration were created with BioRender.com.

Acknowledgment

We would like to thank Christina Gavino for the technical support in inoculating mice and all bacterial analyses. We would also like to thank all members of the Desjardins ASAP team for insightful feedback throughout the course of this study. The study is funded by the joint efforts of The Michael J. Fox Foundation for Parkinson's Research (MJFF) and the Aligning Science Across Parkinson's (ASAP) initiative. MJFF administers the grant ASAP 000525 on behalf of ASAP and itself. SJR received a CIHR-Vanier Canada Graduate Scholarship.

Ethics Statement

The animal study was reviewed and approved by the Université de Montréal Animal Care Use Committee (CDEA) and McGill University Animal Care Committee under conditions specified by the Canadian Council on Animal Care and were approved by.

Author Contributions

SJR led all experiments including, *in vitro*, *in vivo* and bioinformatics work. AK performed flow cytometric staining and analysis of colonic lamina propria cells. HB performed ELISA experiments. BC and JP helped prepared cells for single cell RNAseq while SP and AM helped culture bone marrow-derived cells. SM bred and maintained

animal colony. AA created the website allowing access to and user-friendly analysis of the single cell RNAseq data. EA supported bioinformatics. PT, MD and LET provided feedback on the project. SJR and JAS prepared figures and drafted the manuscript. JAS and SG conceived the project, supervised the work, and approved the final manuscript. All authors contributed to the article and approved the submitted version.

Conflict of Interest

The authors declare that the research was conducted in the absence of any commercial or financial relationships that could be construed as a potential conflict of interest.

Data availability

Raw and processed single cell data available in GEO and source code can be found at https://github.com/stratton-lab/. Raw tabular data of confocal microscopic images available at Zenodo.org. Single cell RNAseq data is accessible through a user-interface website available for further analyses (singlocell.openscience.mcgill.ca/).

Figure legends

Figure 1: Single-cell transcriptomics of the gut in an infection-induced model of Parkinson's disease

A) Lipocalin-2 levels were measured in fecal samples of wild type and PINK1 KO mice at 1-, 2- and 4- w.p.i. and uninfected controls. Two-way ANOVA followed by Tukey's multiple comparison test was applied. Mean ± SEM, n=3-6 mice per group. B) A schematic diagram depicts intestinal infection of wild type and PINK1 KO mice via gavage at 1- and 2-w.p.i. followed by 3' scRNAseq of the colon from 2-3 mice per group. C) Multiple cell types identified in the gut of wild type and PINK1 KO inf. mice and uninf. control groups at 1- and 2-w.p.i. (in red and blue, respectively) are projected in 2D UMAP plots. Each scRNAseq dataset comprises of ~40 000 cells and ~20, 000 genes detected. D) Dotplot indicates the cell identity marker genes curated from the literature used to annotate immune cells in the scRNAseq dataset. E) Integrated UMAP plots of immune cell types across all groups at both timepoints. Weeks post-infection, w.p.i.; knockout, KO; single-cell RNAsequencing, scRNAseq; infected, inf.; uninfected, uninf.; uniform manifold approximation and projection, UMAP.

Figure 2: Differential gene expression analyses of the intestinal immune compartment in an infection-induced PD model before motor symptoms arise

A) UMAP plots of immune cell types in the gut segregated by genotype and timepoint. Note cell populations (in boxes) representing a clear expansion of cell in both genotypes following infection. B) Each heatmap illustrates the number of significant DEGs in each immune cell types of PINK1 KO compared to wild type mice at uninf. 1- and 2-w.p.i. (up- and down-regulated denoted as red and blue, respectively). To test for significance, Wilcoxon Rank Sum test was applied, adjusted p-value < 0.05 using Bonferroni

correction. Helper T cells, Th; cytotoxic 1 T cells, Tc1; naïve T cells, Tn; gamma delta T cells, gdT; natural killer, NK; innate lymphoid cells, ILCs; double-negative T cells, dnT; regulatory T cells, Treg; tissue resident memory, Trm; Differentially expressed genes, DEGs

Figure 3: A larger expansion of proinflammatory and cytotoxic effector T cell subtypes in the gut of PINK1 KO mice following infection

A) Pseudotime analyses of CD4+ and CD8+ T cell subtypes at 2-w.p.i. revealed Th1 to Th17 and Tc1 to Trm lineages from CD4+ and CD8+ Tn, respectively. Both lineages are illustrated in PCA plots of intestinal T cell populations from wild type and PINK1 KO infected mice. B) The proportions of each CD4+ and CD8+ T cell subtypes were assessed and the ratios of Teff-to-Tn in PINK1 KO compared to wild type are quantified. C, D) Pathway enrichment analyses were run on significant DEGs in PINK1 KO CD4+ Th1 and CD8+ Tc1 cells against Gene Ontological terms of biological processes database using *ClusterProfiler*. Dysregulated pathways are shown as treeplots while cnetplots display the genes involved, in which the biological processes and associated genes underlying the activation of adaptive immunity are highlighted in rectangles.
Knockout, KO; helper T cells, Th; cytotoxic 1 T cells, Tc1; naïve T cells, Tn; weeks-post-infection, w.p.i.; tissue resident memory, Trm; effector T cells, Teff

Figure 4: PINK1-driven dysregulation of the myeloid cell lineage at the earliest phase of infection

A) Volcano plots indicating DEGs in PINK1 KO compared to WT of monocytes/macrophages populations at 1- and 2-w.p.i. To test for significance, Wilcoxon Rank Sum test was applied using Bonferroni correction. Significant DEGs (p.adj < 0.5 with a $\log_2$ fold-change ≥ 0.25) are shown in red. B, C) Pathway enrichment analyses were run on significant DEGs at 1-w.p.i. against Gene Ontological terms of biological processes database using *ClusterProfiler*. Dysregulated pathways are shown as a treeplot while a cnetplot display the genes involved. D) Pseudotime analyses of myeloid cell populations at 1-w.p.i. revealed MΦ and DC lineages originating from monocytes, defined by the expression of *Cx3cr1*, *Itgax* and *Ly6c2*, respectively. Both lineages are illustrated in PCA plots of intestinal myeloid cell populations from wild type and PINK1 KO infected mice whereby the monocytes are encircled in red. E, F) The cells within the monocyte population are classified to either immature or mature (MΦ-or DC-like) subtypes with pseudotime values of [0, 10[(low) or [10, 20[(high). The proportions of each monocyte subtypes were assessed and the ratios of MΦ/DC-like-to-immature in PINK1 KO compared to wild type are quantified.

Figure 5: PINK1 KO monocytes acquire enhanced proinflammatory responses

A) Shown is a representative flow cytometric graph of intestinal myeloid cells ($CD45^+CD11b^+$) from wild type and PINK1 KO at 1-w.p.i. $Ly6C^{high}F4/80^-$ monocytes of intestinal myeloid cells were collected by FACS for downstream gene expression analyses by qPCR. B) Expression of key significant DEGs involved in proinflammatory processes identified in monocytes/macrophages cluster were assessed from PINK1 KO infected mice compared to wild type, including *Lcn2*, *Saa3*, *Tlr2*, *Acod1*, *Il10* and *Hif1*α. Two-way ANOVA followed by Tukey's multiple comparison test was applied. Mean ±

SEM, n=3 replicates of 6 pooled mice per group. C) Flow cytometric analyses of Ly6C^{high}F4/80^{-} intestinal monocytes for maturation markers were performed by evaluating geometric mean fluorescent intensity of CD11b and CD11c expressed at high levels in macrophages and dendritic cells. Two-way ANOVA followed by Tukey's multiple comparison test was applied. Mean ± SEM, n=6 mice per group.

Figure 6: Intercellular communication analyses predicted heightened myeloid-cytotoxic CD8+ T cell interactions regulating antigen presentation
A) Unbiased cell-cell interaction analyses of intestinal immune cell populations in wild type and PINK1 KO mice at 1- and 2-w.p.i. was conducted. Analysis of incoming and outgoing interaction strengths showed the putative strongest senders and receivers as the myeloid cells (Mono/MΦ and DC) and effector CD8+ T cells (Tc1 and Trm). B) Chord diagrams illustrate the associations in wild type and PINK1 KO monocytes/macrophages (green) and dendritic cells (blue) to neighboring immune cells at 2-w.p.i. Highlighted in red are pathways underpinning myeloid-CD8+ Tc1 cells interaction, which are relevant to antigen presentation. The width of the arrows symbolizes the number of interactions encompassing the specified pathway. C) Flow cytometric analyses of Ly6C^{high}F4/80^{-} intestinal monocytes were performed and geometric mean fluorescent intensity of proteins related to antigen presentation and implicated in myeloid-CD8 T cells interaction were assessed, including MHCII, CD86, PD-L1 and ICAM1. Two-way ANOVA followed by Tukey's multiple comparison test was applied. Mean ± SEM, n=6 mice per group.

References

Bhatia, D., Grozdanov, V., Ruf, W. P., Kassubek, J., Ludolph, A. C., Weishaupt, J. H., & Danzer, K. M. (2021). T-cell dysregulation is associated with disease severity in Parkinson's Disease. *J Neuroinflammation*, *18*(1), 250. https://doi.org/10.1186/s12974-021-02296-8

Braak, H., Del Tredici, K., Rüb, U., de Vos, R. A., Jansen Steur, E. N., & Braak, E. (2003). Staging of brain pathology related to sporadic Parkinson's disease. *Neurobiol Aging*, *24*(2), 197-211. https://doi.org/10.1016/s0197-4580(02)00065-9

Butler, A., Hoffman, P., Smibert, P., Papalexi, E., & Satija, R. (2018). Integrating single-cell transcriptomic data across different conditions, technologies, and species. *Nat Biotechnol*, *36*(5), 411-420. https://doi.org/10.1038/nbt.4096

Cebrián, C., Zucca, F. A., Mauri, P., Steinbeck, J. A., Studer, L., Scherzer, C. R., Kanter, E., Budhu, S., Mandelbaum, J., Vonsattel, J. P., Zecca, L., Loike, J. D., & Sulzer, D. (2014). MHC-I expression renders catecholaminergic neurons susceptible to T-cell-mediated degeneration. *Nat Commun*, *5*, 3633. https://doi.org/10.1038/ncomms4633

Challis, C., Hori, A., Sampson, T. R., Yoo, B. B., Challis, R. C., Hamilton, A. M., Mazmanian, S. K., Volpicelli-Daley, L. A., & Gradinaru, V. (2020). Gut-seeded α-synuclein fibrils promote gut dysfunction and brain pathology specifically in aged mice. *Nat Neurosci*, *23*(3), 327-336. https://doi.org/10.1038/s41593-020-0589-7

Chandra, R., Sokratian, A., Chavez, K. R., King, S., Swain, S. M., Snyder, J. C., West, A. B., & Liddle, R. A. (2023). Gut mucosal cells transfer α-synuclein to the vagus nerve. *JCI Insight*, *8*(23). https://doi.org/10.1172/jci.insight.172192

Chassaing, B., Srinivasan, G., Delgado, M. A., Young, A. N., Gewirtz, A. T., & Vijay-Kumar, M. (2012). Fecal lipocalin 2, a sensitive and broadly dynamic non-invasive biomarker for intestinal inflammation. *PLoS One*, *7*(9), e44328. https://doi.org/10.1371/journal.pone.0044328

Chen, H., Wang, K., Scheperjans, F., & Killinger, B. (2022). Environmental triggers of Parkinson's disease - Implications of the Braak and dual-hit hypotheses. *Neurobiol Dis*, *163*, 105601. https://doi.org/10.1016/j.nbd.2021.105601

Contento, R. L., Molon, B., Boularan, C., Pozzan, T., Manes, S., Marullo, S., & Viola, A. (2008). CXCR4-CCR5: a couple modulating T cell functions. *Proc Natl Acad Sci U S A*, *105*(29), 10101-10106. https://doi.org/10.1073/pnas.0804286105

Elemeery, M. N., Tchung, A., Boulet, S., Mukherjee, S., Giguère, N., Daudelin, J. F., Even, A., Hétu-Arbour, R., Matheoud, D., Stratton, J. A., Labrecque, N., & Trudeau, L. E. (2024). Adoptive transfer of mitochondrial antigen-specific CD8⁺ T-cells in mice causes parkinsonism and compromises the dopamine system. *bioRxiv*, 2024.2002.2026.582098. https://doi.org/10.1101/2024.02.26.582098

Fahmy, A. M., Cannon, T., Paredes, C. H., Ahmadi, A., Xu, Y. Z., Barette, B., Ibrahim, M., Lanoix, J., Arango-Duque, G., Schurr, E., Chevet, E., Thibault, P., Gruenheid, S., McBride, H., & Desjardins, M. (2023). LRRK2 regulates the activation of the unfolded protein response and antigen presentation in macrophages during inflammation. *bioRxiv*, 2023.2006.2014.545012. https://doi.org/10.1101/2023.06.14.545012

Fan, Y., Li, X., Ma, J., Yang, D., Liang, K., Shen, Y., Wei, W., Dong, L., Liu, C., She, Z., Qi, X., Shi, X., Gu, Q., Zheng, J., & Li, D. (2024). Increased plasma lipocalin-2 levels are associated with nonmotor symptoms and neuroimaging features in patients with Parkinson's disease. *J Neurosci Res*, *102*(2), e25303. https://doi.org/10.1002/jnr.25303

Farmen, K., Nissen, S. K., Stokholm, M. G., Iranzo, A., Østergaard, K., Serradell, M., Otto, M., Svendsen, K. B., Garrido, A., Vilas, D., Borghammer, P., Santamaria, J., Møller, A., Gaig, C., Brooks, D. J., Tolosa, E., Pavese, N., & Romero-Ramos, M. (2021). Monocyte markers correlate with immune and neuronal brain changes in REM sleep behavior disorder. *Proc Natl Acad Sci U S A*, *118*(10). https://doi.org/10.1073/pnas.2020858118

Fava, V. M., Xu, Y. Z., Lettre, G., Van Thuc, N., Orlova, M., Thai, V. H., Tao, S., Croteau, N., Eldeeb, M. A., MacDougall, E. J., Cambri, G., Lahiri, R., Adams, L., Fon, E. A., Trempe, J. F., Cobat, A., Alcaïs, A., Abel, L., & Schurr, E. (2019). Pleiotropic effects for Parkin and LRRK2 in leprosy type-1 reactions and Parkinson's disease. *Proc Natl Acad Sci U S A*, *116*(31), 15616-15624. https://doi.org/10.1073/pnas.1901805116

Fu, P., Gao, M., & Yung, K. K. L. (2020). Association of Intestinal Disorders with Parkinson's Disease and Alzheimer's Disease: A Systematic Review and Meta-Analysis. *ACS Chem Neurosci*, *11*(3), 395-405. https://doi.org/10.1021/acschemneuro.9b00607

Galiano-Landeira, J., Torra, A., Vila, M., & Bové, J. (2020). CD8 T cell nigral infiltration precedes synucleinopathy in early stages of Parkinson's disease. *Brain*, *143*(12), 3717-3733. https://doi.org/10.1093/brain/awaa269

Härtlova, A., Herbst, S., Peltier, J., Rodgers, A., Bilkei-Gorzo, O., Fearns, A., Dill, B. D., Lee, H., Flynn, R., Cowley, S. A., Davies, P., Lewis, P. A., Ganley, I. G., Martinez, J., Alessi, D. R., Reith, A. D., Trost, M., & Gutierrez, M. G. (2018). LRRK2 is a negative regulator of Mycobacterium tuberculosis phagosome maturation in macrophages. *Embo j*, *37*(12). https://doi.org/10.15252/embj.201798694

Heo, J. M., Ordureau, A., Paulo, J. A., Rinehart, J., & Harper, J. W. (2015). The PINK1-PARKIN Mitochondrial Ubiquitylation Pathway Drives a Program of OPTN/NDP52 Recruitment and TBK1 Activation to Promote Mitophagy. *Mol Cell*, *60*(1), 7-20. https://doi.org/10.1016/j.molcel.2015.08.016

Hor, J. W., Lim, S. Y., Khor, E. S., Chong, K. K., Song, S. L., Ibrahim, N. M., Teh, C. S. J., Chong, C. W., Hilmi, I. N., & Tan, A. H. (2022). Fecal Calprotectin in Parkinson's Disease and Multiple System Atrophy. *J Mov Disord*, *15*(2), 106-114. https://doi.org/10.14802/jmd.21085

Houser, M. C., Chang, J., Factor, S. A., Molho, E. S., Zabetian, C. P., Hill-Burns, E. M., Payami, H., Hertzberg, V. S., & Tansey, M. G. (2018). Stool Immune Profiles Evince Gastrointestinal Inflammation in Parkinson's Disease. *Mov Disord*, *33*(5), 793-804. https://doi.org/10.1002/mds.27326

Jakubiak, K., Paryani, F., Kannan, A., Lee, J., Madden, N., Li, J., Chen, D., Mahajan, A., Xia, S., Flowers, X., Menon, V., Sulzer, D., Goldman, J., Sims, P. A., & Al-Dalahmah, O. (2024). The spatial landscape of glial pathology and T-cell response in Parkinson’s disease substantia nigra. *bioRxiv*, 2024.2001.2008.574736. https://doi.org/10.1101/2024.01.08.574736

Jin, S., Guerrero-Juarez, C. F., Zhang, L., Chang, I., Ramos, R., Kuan, C. H., Myung, P., Plikus, M. V., & Nie, Q. (2021). Inference and analysis of cell-cell communication using CellChat. *Nat Commun*, *12*(1), 1088. https://doi.org/10.1038/s41467-021-21246-9

Jin, U., Park, S. J., Lee, B. G., Kim, J. B., Kim, S. J., Joe, E. H., Woo, H. G., & Park, S. M. (2023). Critical roles of parkin and PINK1 in coxsackievirus B3-induced viral myocarditis. *Microbes Infect*, *25*(8), 105211. https://doi.org/10.1016/j.micinf.2023.105211

Kazanova, A., Sung, J., Oliveira, N., Gavino, C., Recinto, S., Bessaiah, H., Pei, J., Burns, L., Miller, W., Brouillard-Galipeau, M., Zhu, L., Guerra, L., Elemeery, M. N., MacDonald, A., Lanoix, J., Thibault, P., McBride, H., Desjardins, M., Stratton, J. A., . . . Gruenheid, S. (2024). Modeling gene-environment interactions in Parkinson’s Disease: Helicobacter pylori infection of Pink1^{−/−} mice induces CD8 T cell-dependent motor and cognitive dysfunction. *bioRxiv*, 2024.2002.2025.580545. https://doi.org/10.1101/2024.02.25.580545

Kim, S., Kwon, S. H., Kam, T. I., Panicker, N., Karuppagounder, S. S., Lee, S., Lee, J. H., Kim, W. R., Kook, M., Foss, C. A., Shen, C., Lee, H., Kulkarni, S., Pasricha, P. J., Lee, G., Pomper, M. G., Dawson, V. L., Dawson, T. M., & Ko, H. S. (2019). Transneuronal Propagation of Pathologic α-Synuclein from the Gut to the Brain

Models Parkinson's Disease. *Neuron*, *103*(4), 627-641.e627. https://doi.org/10.1016/j.neuron.2019.05.035

Kimura, K., Nishigori, R., Hamatani, M., Sawamura, M., Ashida, S., Fujii, C., Takata, M., Lin, Y., Sato, W., Okamoto, T., Kuzuya, A., Takahashi, R., Yamamura, T., & Kondo, T. (2024). Resident Memory-like CD8(+) T Cells Are Involved in Chronic Inflammatory and Neurodegenerative Diseases in the CNS. *Neurol Neuroimmunol Neuroinflamm*, *11*(1). https://doi.org/10.1212/nxi.0000000000200172

Lazarou, M., Sliter, D. A., Kane, L. A., Sarraf, S. A., Wang, C., Burman, J. L., Sideris, D. P., Fogel, A. I., & Youle, R. J. (2015). The ubiquitin kinase PINK1 recruits autophagy receptors to induce mitophagy. *Nature*, *524*(7565), 309-314. https://doi.org/10.1038/nature14893

Lee, H. S., Lobbestael, E., Vermeire, S., Sabino, J., & Cleynen, I. (2021). Inflammatory bowel disease and Parkinson's disease: common pathophysiological links. *Gut*, *70*(2), 408-417. https://doi.org/10.1136/gutjnl-2020-322429

Li, J., Ma, C., Long, F., Yang, D., Liu, X., Hu, Y., Wu, C., Wang, B., Wang, M., Chen, Y., Liu, G., Moynagh, P. N., Zhou, J., Peng, T., & Yang, S. (2019). Parkin Impairs Antiviral Immunity by Suppressing the Mitochondrial Reactive Oxygen Species-Nlrp3 Axis and Antiviral Inflammation. *iScience*, *16*, 468-484. https://doi.org/10.1016/j.isci.2019.06.008

Lindestam Arlehamn, C. S., Dhanwani, R., Pham, J., Kuan, R., Frazier, A., Rezende Dutra, J., Phillips, E., Mallal, S., Roederer, M., Marder, K. S., Amara, A. W., Standaert, D. G., Goldman, J. G., Litvan, I., Peters, B., Sulzer, D., & Sette, A. (2020). α-Synuclein-specific T cell reactivity is associated with preclinical and early Parkinson's disease. *Nat Commun*, *11*(1), 1875. https://doi.org/10.1038/s41467-020-15626-w

Liu, B., Gao, H. M., & Hong, J. S. (2003). Parkinson's disease and exposure to infectious agents and pesticides and the occurrence of brain injuries: role of neuroinflammation. *Environ Health Perspect*, *111*(8), 1065-1073. https://doi.org/10.1289/ehp.6361

Liu, W., Liu, X., Li, Y., Zhao, J., Liu, Z., Hu, Z., Wang, Y., Yao, Y., Miller, A. W., Su, B., Cookson, M. R., Li, X., & Kang, Z. (2017). LRRK2 promotes the activation of NLRC4 inflammasome during Salmonella Typhimurium infection. *J Exp Med*, *214*(10), 3051-3066. https://doi.org/10.1084/jem.20170014

Matheoud, D., Cannon, T., Voisin, A., Penttinen, A. M., Ramet, L., Fahmy, A. M., Ducrot, C., Laplante, A., Bourque, M. J., Zhu, L., Cayrol, R., Le Campion, A., McBride, H. M., Gruenheid, S., Trudeau, L. E., & Desjardins, M. (2019). Intestinal infection triggers Parkinson's disease-like symptoms in Pink1(-/-) mice. *Nature*, *571*(7766), 565-569. https://doi.org/10.1038/s41586-019-1405-y

Matheoud, D., Sugiura, A., Bellemare-Pelletier, A., Laplante, A., Rondeau, C., Chemali, M., Fazel, A., Bergeron, J. J., Trudeau, L. E., Burelle, Y., Gagnon, E., McBride, H. M., & Desjardins, M. (2016). Parkinson's Disease-Related Proteins PINK1 and Parkin Repress Mitochondrial Antigen Presentation. *Cell*, *166*(2), 314-327. https://doi.org/10.1016/j.cell.2016.05.039

Mulak, A., Koszewicz, M., Panek-Jeziorna, M., Koziorowska-Gawron, E., & Budrewicz, S. (2019). Fecal Calprotectin as a Marker of the Gut Immune System Activation

Is Elevated in Parkinson's Disease. *Front Neurosci*, *13*, 992. https://doi.org/10.3389/fnins.2019.00992

Mullineaux-Sanders, C., Sanchez-Garrido, J., Hopkins, E. G. D., Shenoy, A. R., Barry, R., & Frankel, G. (2019). Citrobacter rodentium-host-microbiota interactions: immunity, bioenergetics and metabolism. *Nat Rev Microbiol*, *17*(11), 701-715. https://doi.org/10.1038/s41579-019-0252-z

Nerius, M., Doblhammer, G., & Tamgüney, G. (2020). GI infections are associated with an increased risk of Parkinson's disease. *Gut*, *69*(6), 1154-1156. https://doi.org/10.1136/gutjnl-2019-318822

Nguyen, M., Collier, J. J., Ignatenko, O., Morin, G., Huang, S., Desjardins, M., & McBride, H. M. (2023). Parkinson's genes orchestrate pyroptosis through selective trafficking of mtDNA to leaky lysosomes. *bioRxiv*, 2023.2009.2011.557213. https://doi.org/10.1101/2023.09.11.557213

Oh, S. J., Yu, J. W., Ahn, J. H., Choi, S. T., Park, H., Yun, J., & Shin, O. S. (2024). Varicella zoster virus glycoprotein E facilitates PINK1/Parkin-mediated mitophagy to evade STING and MAVS-mediated antiviral innate immunity. *Cell Death Dis*, *15*(1), 16. https://doi.org/10.1038/s41419-023-06400-z

Parkinson's disease: Prevalence, diagnosis and impact. (2015). Government of Canada, Statistics Canada. Retrieved June 9 from https://www150.statcan.gc.ca/n1/pub/82-003-x/2014011/article/14112-eng.htm

Pickrell, A. M., & Youle, R. J. (2015). The roles of PINK1, parkin, and mitochondrial fidelity in Parkinson's disease. *Neuron*, *85*(2), 257-273. https://doi.org/10.1016/j.neuron.2014.12.007

Requejo-Aguilar, R., Lopez-Fabuel, I., Fernandez, E., Martins, L. M., Almeida, A., & Bolaños, J. P. (2014). PINK1 deficiency sustains cell proliferation by reprogramming glucose metabolism through HIF1. *Nat Commun*, *5*, 4514. https://doi.org/10.1038/ncomms5514

Sampson, T. R., Challis, C., Jain, N., Moiseyenko, A., Ladinsky, M. S., Shastri, G. G., Thron, T., Needham, B. D., Horvath, I., Debelius, J. W., Janssen, S., Knight, R., Wittung-Stafshede, P., Gradinaru, V., Chapman, M., & Mazmanian, S. K. (2020). A gut bacterial amyloid promotes α-synuclein aggregation and motor impairment in mice. *Elife*, *9*. https://doi.org/10.7554/eLife.53111

Sampson, T. R., Debelius, J. W., Thron, T., Janssen, S., Shastri, G. G., Ilhan, Z. E., Challis, C., Schretter, C. E., Rocha, S., Gradinaru, V., Chesselet, M. F., Keshavarzian, A., Shannon, K. M., Krajmalnik-Brown, R., Wittung-Stafshede, P., Knight, R., & Mazmanian, S. K. (2016). Gut Microbiota Regulate Motor Deficits and Neuroinflammation in a Model of Parkinson's Disease. *Cell*, *167*(6), 1469-1480.e1412. https://doi.org/10.1016/j.cell.2016.11.018

Schröder, J. B., Pawlowski, M., Meyer Zu Hörste, G., Gross, C. C., Wiendl, H., Meuth, S. G., Ruck, T., & Warnecke, T. (2018). Immune Cell Activation in the Cerebrospinal Fluid of Patients With Parkinson's Disease. *Front Neurol*, *9*, 1081. https://doi.org/10.3389/fneur.2018.01081

Schwiertz, A., Spiegel, J., Dillmann, U., Grundmann, D., Bürmann, J., Faßbender, K., Schäfer, K. H., & Unger, M. M. (2018). Fecal markers of intestinal inflammation and intestinal permeability are elevated in Parkinson's disease. *Parkinsonism Relat Disord*, *50*, 104-107. https://doi.org/10.1016/j.parkreldis.2018.02.022

Shen, X., Yang, H., Wu, Y., Zhang, D., & Jiang, H. (2017). Meta-analysis: Association of Helicobacter pylori infection with Parkinson's diseases. *Helicobacter*, *22*(5). https://doi.org/10.1111/hel.12398

Sliter, D. A., Martinez, J., Hao, L., Chen, X., Sun, N., Fischer, T. D., Burman, J. L., Li, Y., Zhang, Z., Narendra, D. P., Cai, H., Borsche, M., Klein, C., & Youle, R. J. (2018). Parkin and PINK1 mitigate STING-induced inflammation. *Nature*, *561*(7722), 258-262. https://doi.org/10.1038/s41586-018-0448-9

Smith, A. M., Depp, C., Ryan, B. J., Johnston, G. I., Alegre-Abarrategui, J., Evetts, S., Rolinski, M., Baig, F., Ruffmann, C., Simon, A. K., Hu, M. T. M., & Wade-Martins, R. (2018). Mitochondrial dysfunction and increased glycolysis in prodromal and early Parkinson's blood cells. *Mov Disord*, *33*(10), 1580-1590. https://doi.org/10.1002/mds.104

Stallhofer, J., Friedrich, M., Konrad-Zerna, A., Wetzke, M., Lohse, P., Glas, J., Tillack-Schreiber, C., Schnitzler, F., Beigel, F., & Brand, S. (2015). Lipocalin-2 Is a Disease Activity Marker in Inflammatory Bowel Disease Regulated by IL-17A, IL-22, and TNF-α and Modulated by IL23R Genotype Status. *Inflamm Bowel Dis*, *21*(10), 2327-2340. https://doi.org/10.1097/mib.0000000000000515

Sulzer, D., Alcalay, R. N., Garretti, F., Cote, L., Kanter, E., Agin-Liebes, J., Liong, C., McMurtrey, C., Hildebrand, W. H., Mao, X., Dawson, V. L., Dawson, T. M., Oseroff, C., Pham, J., Sidney, J., Dillon, M. B., Carpenter, C., Weiskopf, D., Phillips, E., . . . Sette, A. (2017). T cells from patients with Parkinson's disease recognize α-synuclein peptides. *Nature*, *546*(7660), 656-661. https://doi.org/10.1038/nature22815

Sun, L., Shen, R., Agnihotri, S. K., Chen, Y., Huang, Z., & Büeler, H. (2018). Lack of PINK1 alters glia innate immune responses and enhances inflammation-induced, nitric oxide-mediated neuron death. *Sci Rep*, *8*(1), 383. https://doi.org/10.1038/s41598-017-18786-w

Sun, M. F., Zhu, Y. L., Zhou, Z. L., Jia, X. B., Xu, Y. D., Yang, Q., Cui, C., & Shen, Y. Q. (2018). Neuroprotective effects of fecal microbiota transplantation on MPTP-induced Parkinson's disease mice: Gut microbiota, glial reaction and TLR4/TNF-α signaling pathway. *Brain Behav Immun*, *70*, 48-60. https://doi.org/10.1016/j.bbi.2018.02.005

Sung, H. Y., Choi, M. G., Kim, Y. I., Lee, K. S., & Kim, J. S. (2012). Anorectal manometric dysfunctions in newly diagnosed, early-stage Parkinson's disease. *J Clin Neurol*, *8*(3), 184-189. https://doi.org/10.3988/jcn.2012.8.3.184

Tysnes, O. B., & Storstein, A. (2017). Epidemiology of Parkinson's disease. *J Neural Transm (Vienna)*, *124*(8), 901-905. https://doi.org/10.1007/s00702-017-1686-y

Wang, L., Yukselten, Y., Nuwagaba, J., & Sutton, R. E. (2024). JAK/STAT signaling pathway affects CCR5 expression in human CD4(+) T cells. *Sci Adv*, *10*(12), eadl0368. https://doi.org/10.1126/sciadv.adl0368

Wang, P., Yao, L., Luo, M., Zhou, W., Jin, X., Xu, Z., Yan, S., Li, Y., Xu, C., Cheng, R., Huang, Y., Lin, X., Ma, K., Cao, H., Liu, H., Xue, G., Han, F., Nie, H., & Jiang, Q. (2021). Single-cell transcriptome and TCR profiling reveal activated and expanded T cell populations in Parkinson's disease. *Cell Discov*, *7*(1), 52. https://doi.org/10.1038/s41421-021-00280-3

Wijeyekoon, R. S., Kronenberg-Versteeg, D., Scott, K. M., Hayat, S., Kuan, W. L., Evans, J. R., Breen, D. P., Cummins, G., Jones, J. L., Clatworthy, M. R., Floto, R. A., Barker, R. A., & Williams-Gray, C. H. (2020). Peripheral innate immune and bacterial signals relate to clinical heterogeneity in Parkinson's disease. *Brain Behav Immun*, *87*, 473-488. https://doi.org/10.1016/j.bbi.2020.01.018

Williams, G. P., Michaelis, T., Lima-Junior, J. R., Frazier, A., Tran, N. K., Phillips, E. J., Mallal, S. A., Litvan, I., Goldman, J. G., Alcalay, R. N., Sidney, J., Sulzer, D., Sette, A., & Lindestam Arlehamn, C. S. (2024). PINK1 is a target of T cell responses in Parkinson's disease. *bioRxiv*. https://doi.org/10.1101/2024.02.09.579465

Xin, D., Gu, H., Liu, E., & Sun, Q. (2018). Parkin negatively regulates the antiviral signaling pathway by targeting TRAF3 for degradation. *J Biol Chem*, *293*(31), 11996-12010. https://doi.org/10.1074/jbc.RA117.001201

Zhong, Z., Chen, W., Gao, H., Che, N., Xu, M., Yang, L., Zhang, Y., & Ye, M. (2021). Fecal Microbiota Transplantation Exerts a Protective Role in MPTP-Induced Parkinson's Disease via the TLR4/PI3K/AKT/NF-κB Pathway Stimulated by α-Synuclein. *Neurochem Res*, *46*(11), 3050-3058. https://doi.org/10.1007/s11064-021-03411-0

Zhou, J., Yang, R., Zhang, Z., Liu, Q., Zhang, Y., Wang, Q., & Yuan, H. (2019). Mitochondrial Protein PINK1 Positively Regulates RLR Signaling. *Front Immunol*, *10*, 1069. https://doi.org/10.3389/fimmu.2019.01069

Figure 1: Single-cell transcriptomics of the gut in an infection-induced model of Parkinson's disease

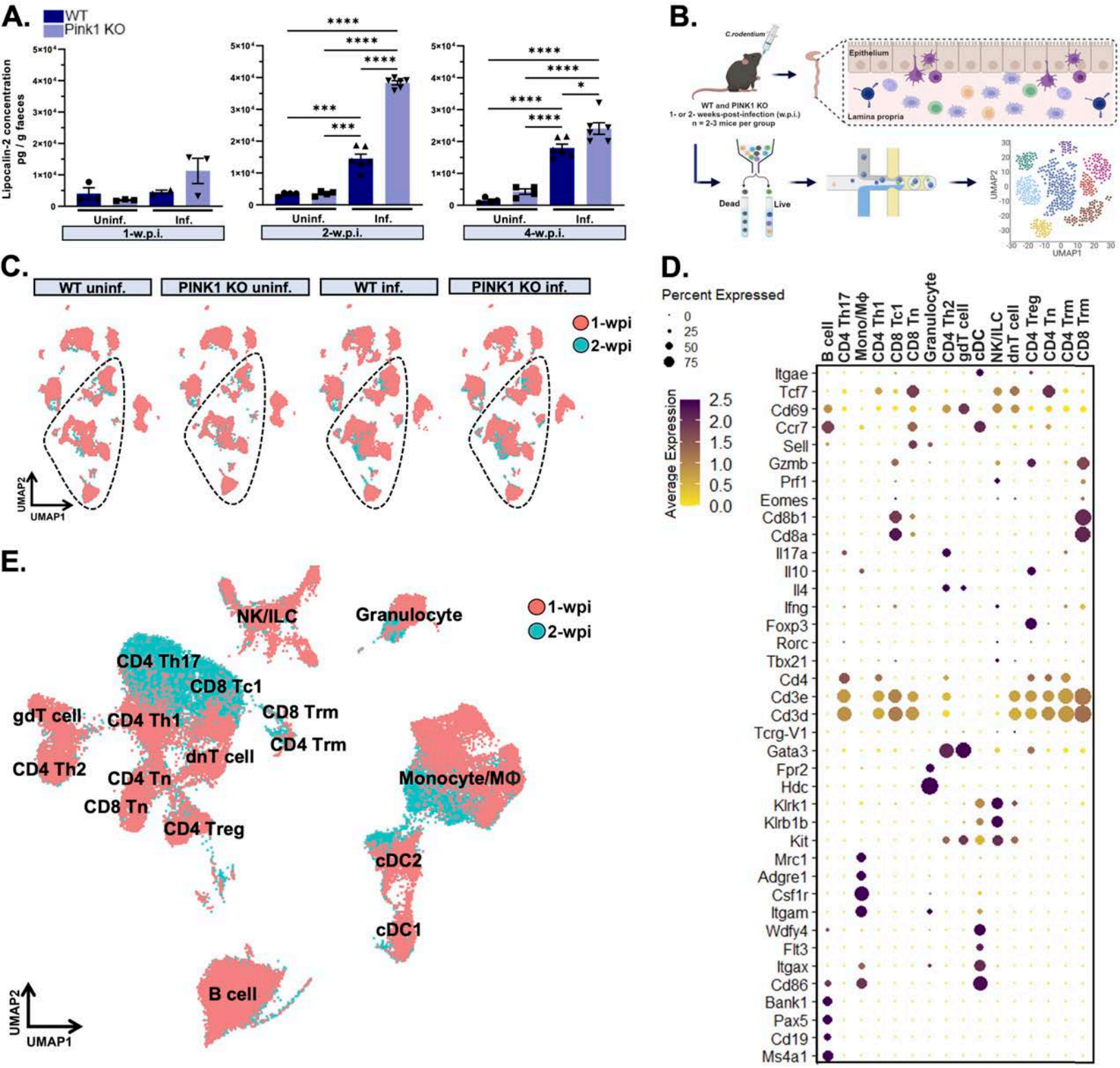

Figure 2: Differential gene expression analyses of the intestinal immune compartment in an infection-induced PD model before motor symptoms arise

A.

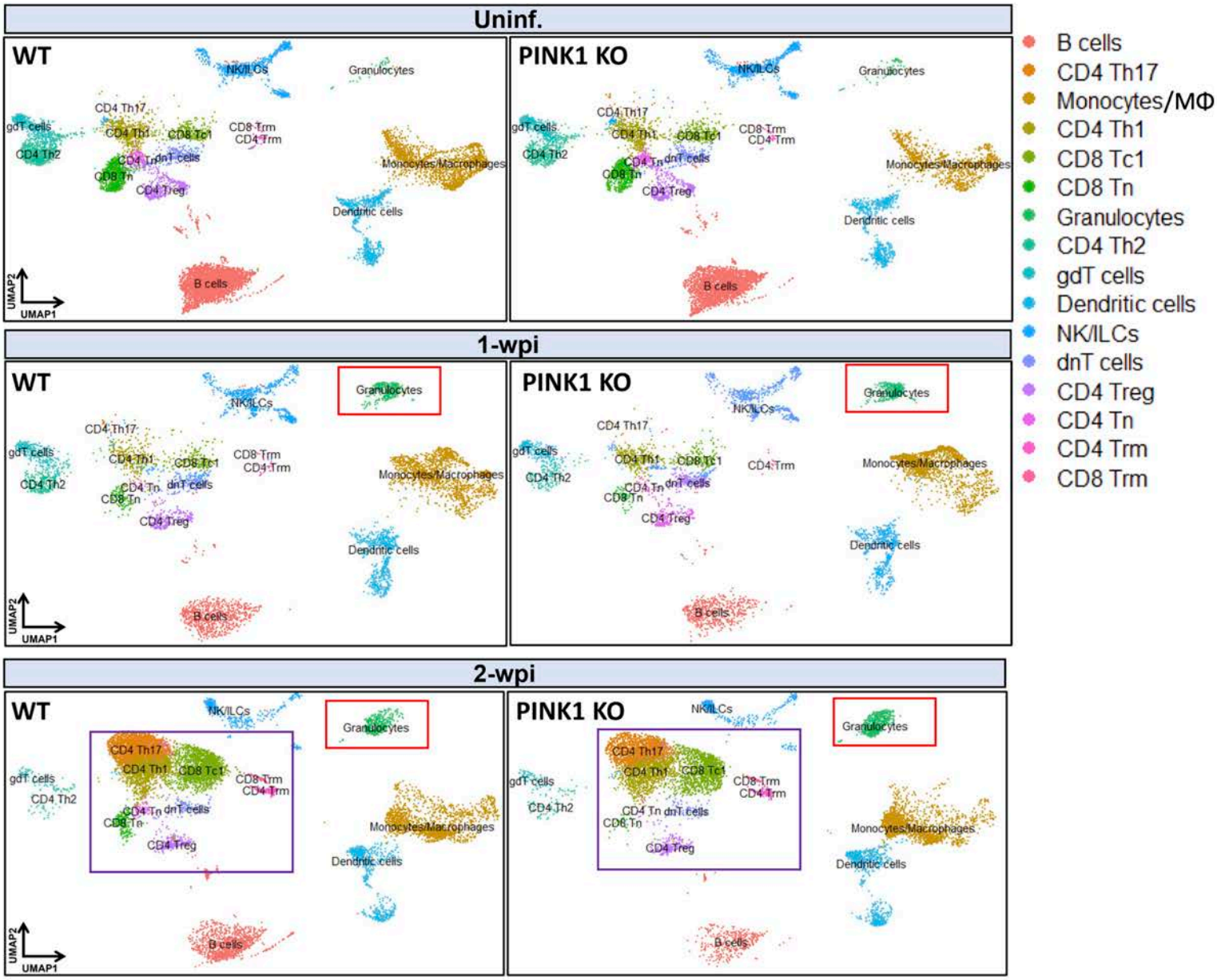

B.

	Mono/ Mϕ	cDC	Gran	NK/ ILC	BC	gdT	dnT	CD4 Tn	CD4 Trm	CD4 Th1	CD4 Th2	CD4 Th17	CD4 Treg	CD8 Tn	CD8 Trm	CD8 Tc1
Uninf.	3	1	0	1	12	1	1	0	0	1	2	0	1	5	0	1
Uninf.	4	4	0	4	13	2	0	1	0	2	3	0	2	5	0	1
1-wpi	343	72	12	56	35	20	14	0	0	18	16	0	14	5	5	8
1-wpi	248	92	30	43	43	9	9	0	0	13	12	0	3	2	2	4
2-wpi	107	25	7	7	15	1	0	1	6	34	1	63	6	2	1	43
2-wpi	180	32	26	9	39	1	1	1	6	107	0	121	3	1	2	72

CD4 CD8

Upregulated in PINK1KO (p-adj<0.05) 300 100

Downregulated in PINK1KO (p-adj<0.05) 300 100

Figure 3: A larger expansion of proinflammatory and cytotoxic effector T cell subtypes in the gut of PINK1 KO mice following infection

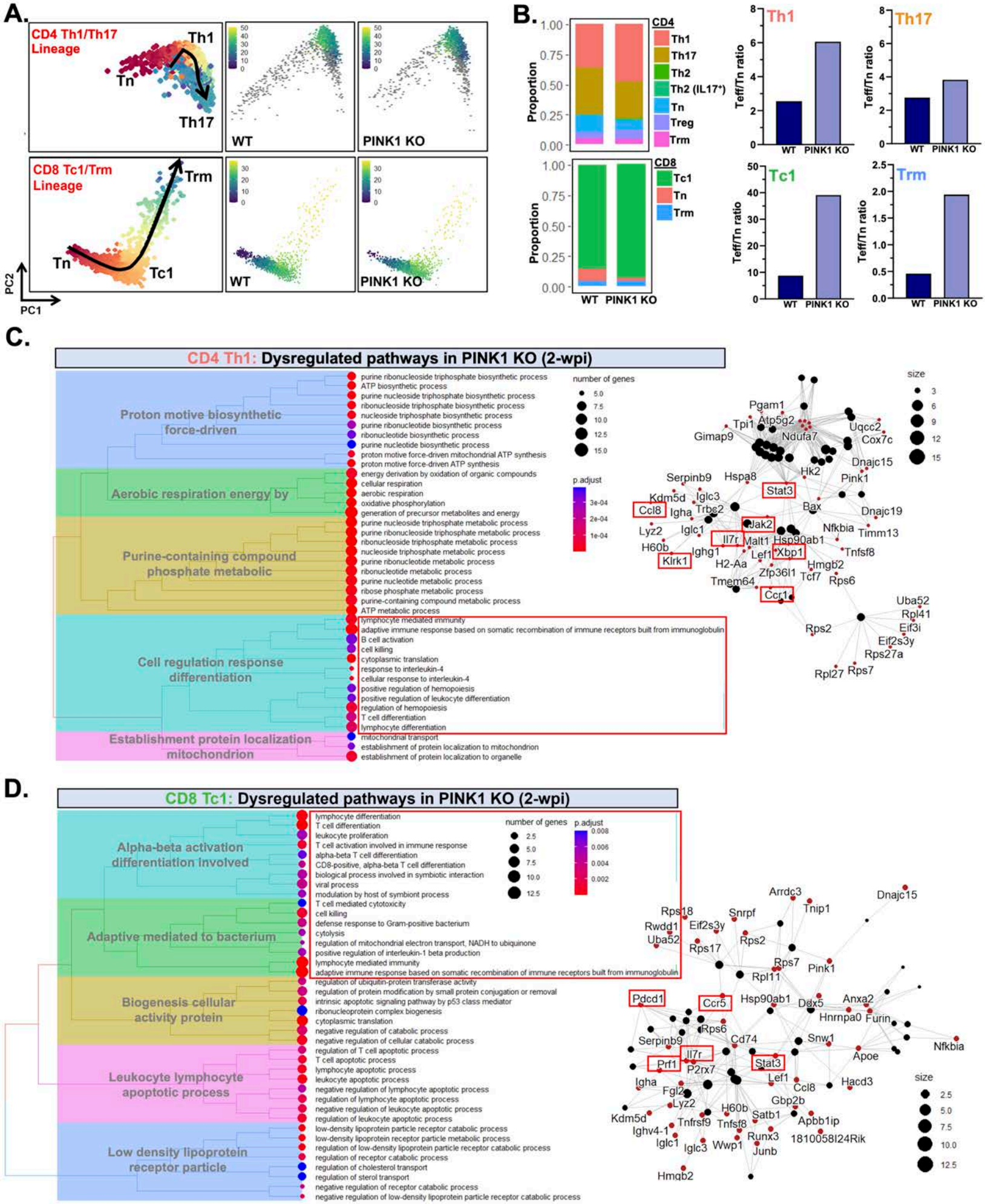

Figure 4: PINK1-driven dysregulation of the myeloid cell lineage at the earliest phase of disease

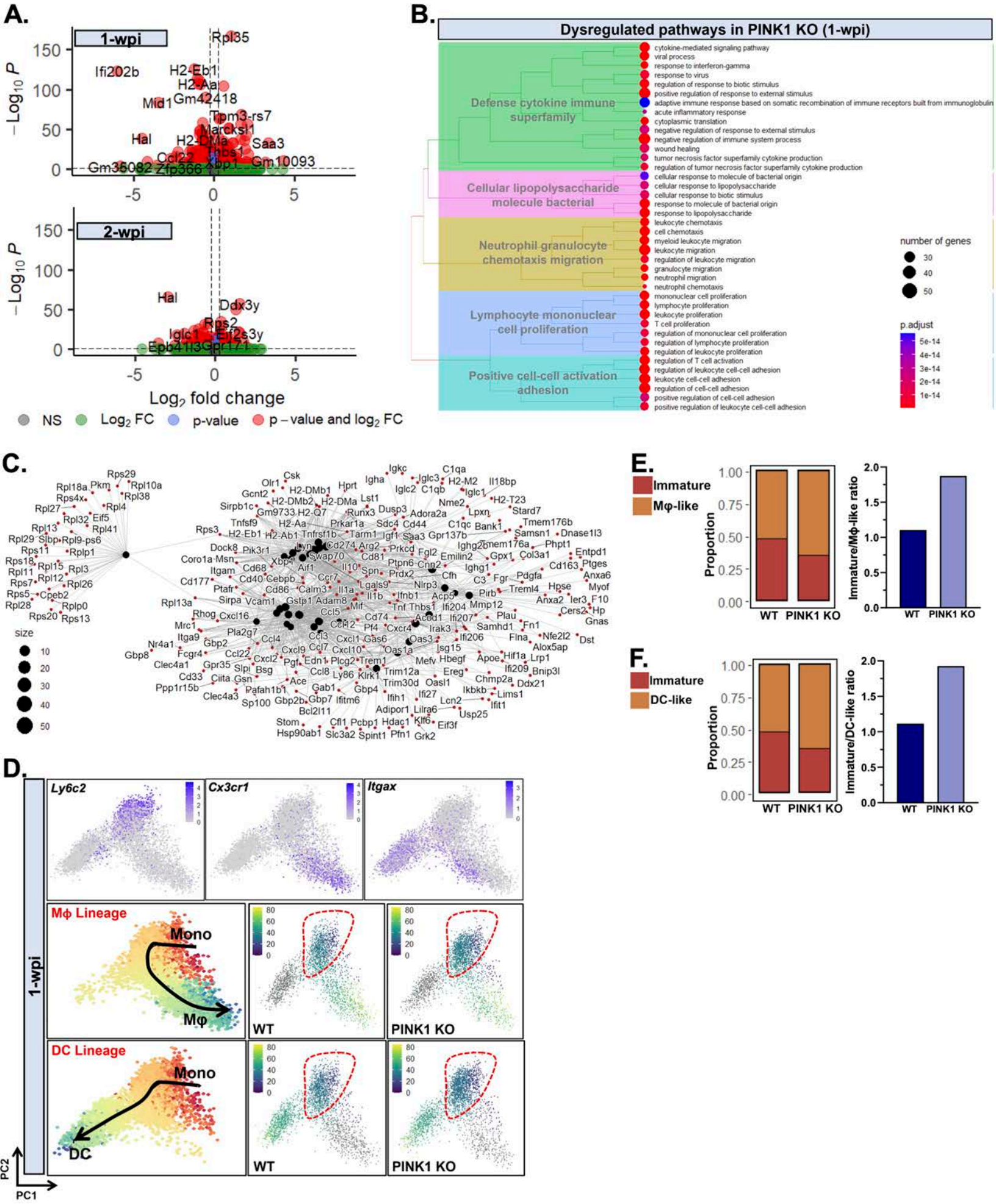

Figure 5: PINK1 KO monocytes acquire enhanced proinflammatory responses

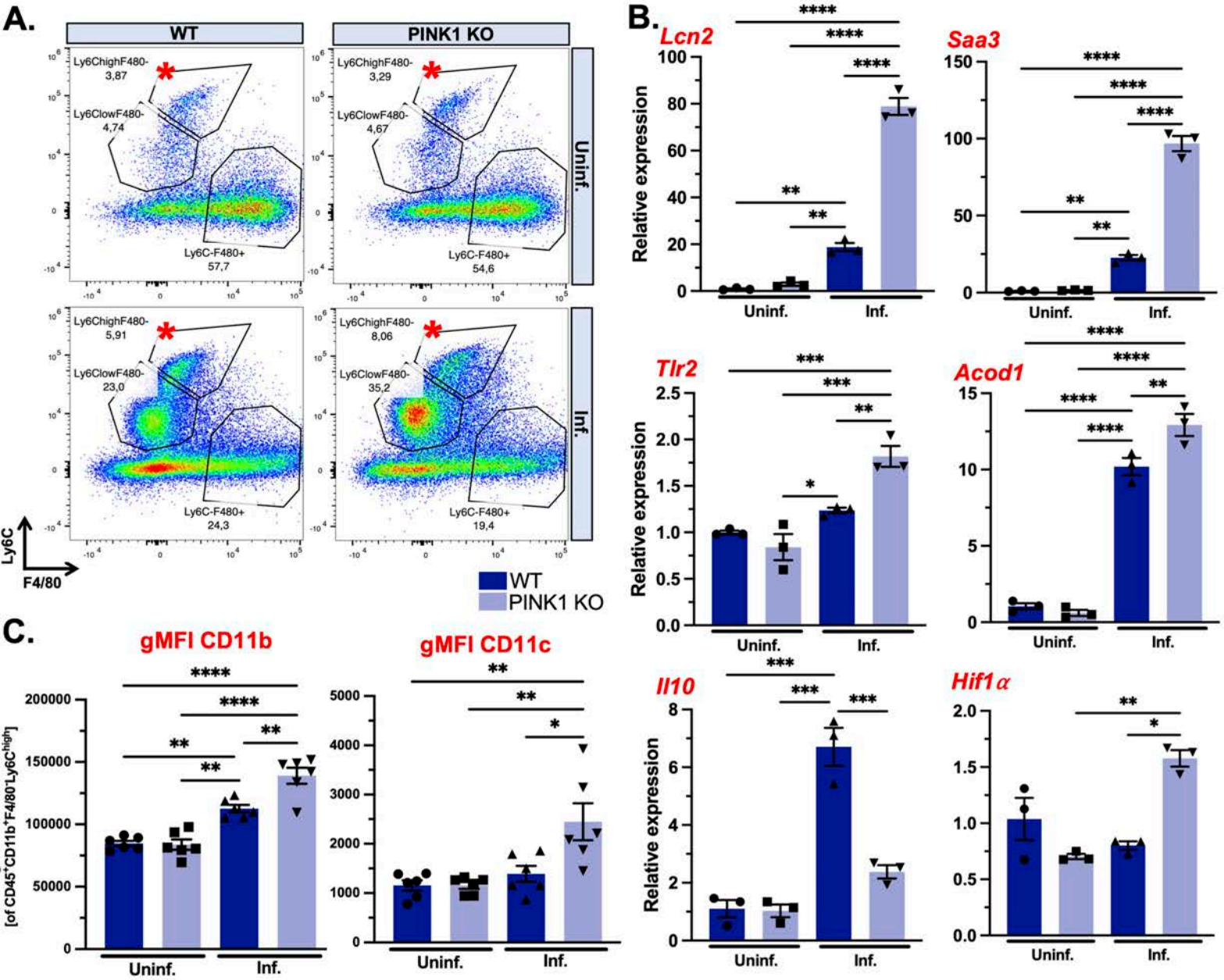
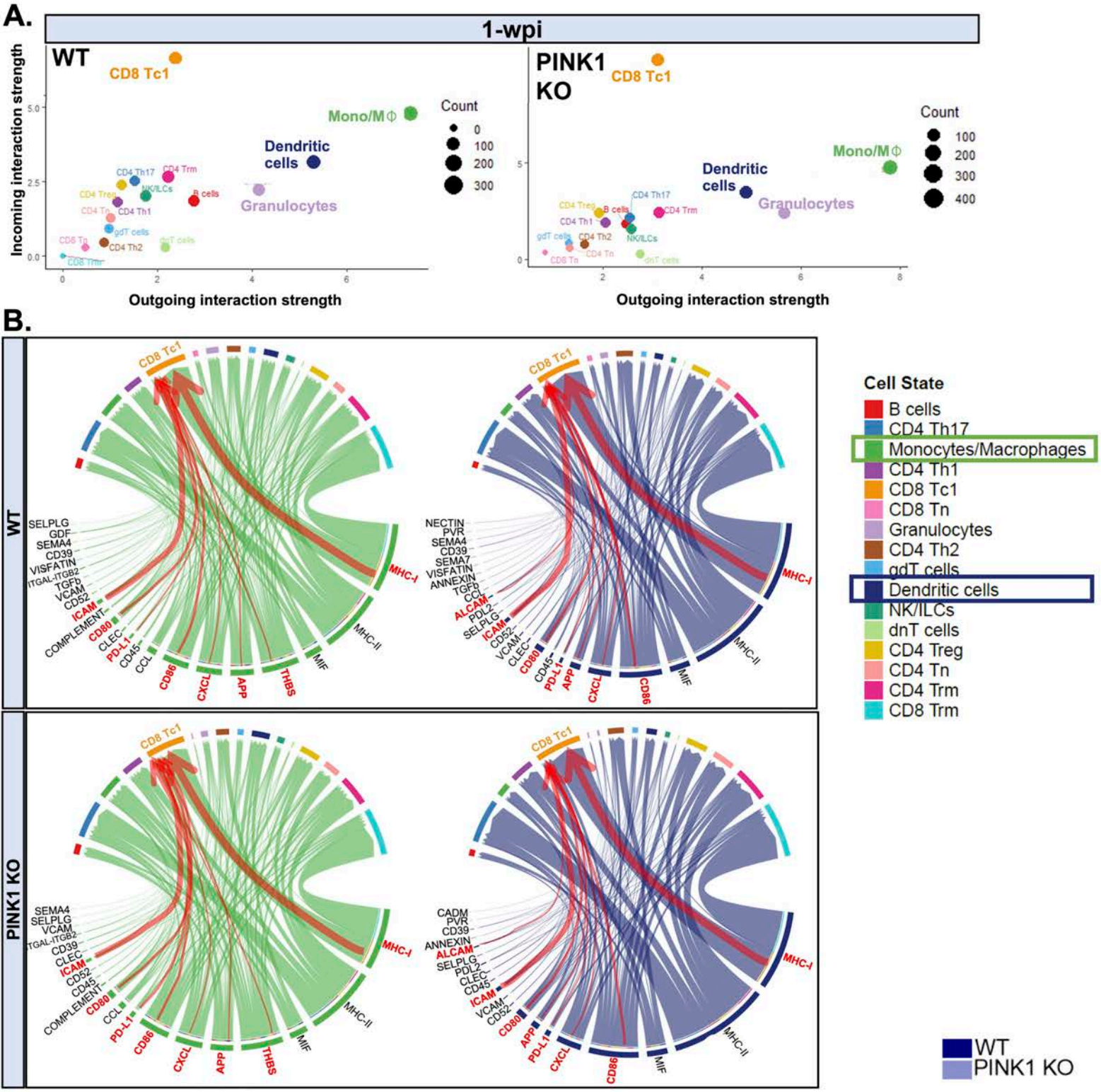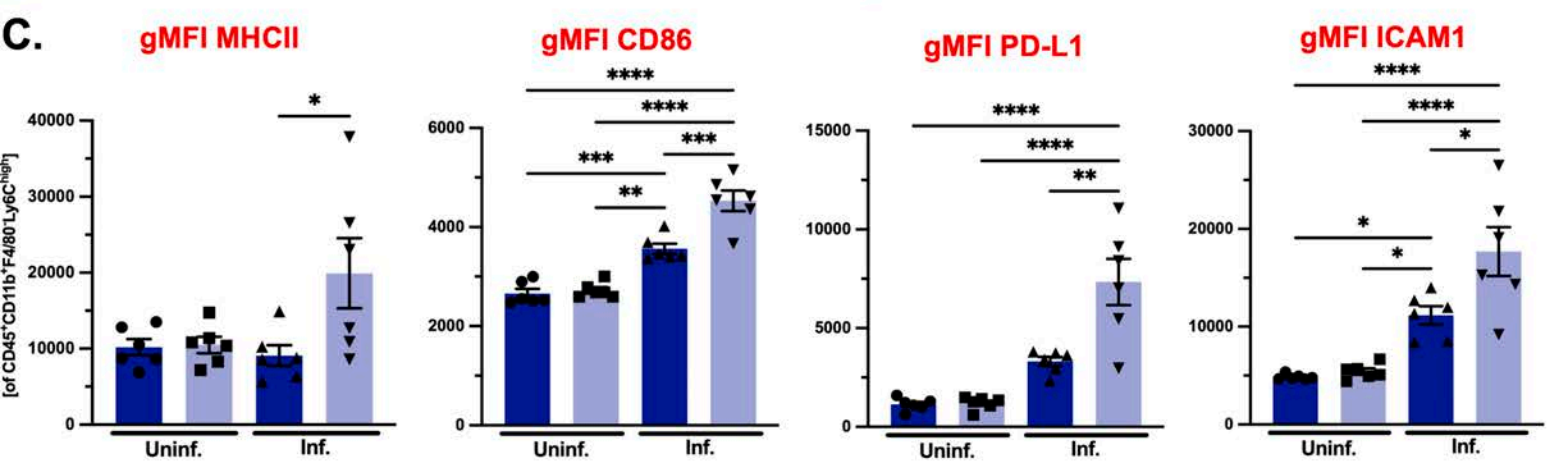
Figure 6: Intercellular communication analyses predicted heightened myeloid-cytotoxic CD8 T cell interactions regulating antigen presentation